nature neuroscience

A new type of microglia gene targeting shows TAK1 to be pivotal in CNS autoimmune inflammation

Tobias Goldmann[1,7], Peter Wieghofer[1,2,7], Philippe F Müller[1], Yochai Wolf[3], Diana Varol[3], Simon Yona[3], Stefanie M Brendecke[1], Katrin Kierdorf[1], Ori Staszewski[1], Moumita Datta[1], Tom Luedde[4], Mathias Heikenwalder[5], Steffen Jung[3,7] & Marco Prinz[1,6,7]

Microglia are brain macrophages and, as such, key immune-competent cells that can respond to environmental changes. Understanding the mechanisms of microglia-specific responses during pathologies is hence vital for reducing disease burden. The definition of microglial functions has so far been hampered by the lack of genetic *in vivo* approaches that allow discrimination of microglia from closely related peripheral macrophage populations in the body. Here we introduce a mouse experimental system that specifically targets microglia to examine the role of a mitogen-associated protein kinase kinase kinase (MAP3K), transforming growth factor (TGF)-β-activated kinase 1 (TAK1), during autoimmune inflammation. Conditional depletion of TAK1 in microglia only, not in neuroectodermal cells, suppressed disease, significantly reduced CNS inflammation and diminished axonal and myelin damage by cell-autonomous inhibition of the NF-κB, JNK and ERK1/2 pathways. Thus, we found TAK1 to be pivotal in CNS autoimmunity, and we present a tool for future investigations of microglial function in the CNS.

Microglia are the brain endogenous macrophages, crucially involved in the scavenging of dying cells, pathogens and molecules that engage pattern recognition receptors, leading to subsequent activation of immune molecules and induction of phagocytosis and endocytosis[1,2]. In contrast to other brain cells, such as neurons, astrocytes and oligodendrocytes, microglia belong to the mononuclear phagocytic system of the body, which is derived from progenitors of the primitive hematopoiesis in the yolk sac during early embryogenesis[3–6].

As key immune effector cells of the CNS, surveillant microglia are distributed throughout the brain and act as sensors of pathologic events. Although microglial activation has been described extensively in many CNS diseases, its impact on disease pathogenesis remains ill-defined[7]. In autoimmune diseases such as multiple sclerosis, most data point to detrimental roles of microglia—for example, by their production of neurotoxic molecules, proinflammatory cytokines or chemokines, or by presenting self-antigens[8–10]. But there have also been claims that microglial activation counteracts pathologic processes in other diseases by providing neurotrophic or immunosuppressive factors[11,12].

Furthermore, recent experiments suggest that microglia also support and monitor normal synaptic function[13], control synaptogenesis[14] and induce developmental apoptosis of Purkinje cells *in vitro*[15]. The role of microglia in maintaining brain homeostasis was recently demonstrated in mental disorders such as Rett syndrome, a neurodevelopmental disease caused by mutation of the gene encoding methyl-CpG binding protein (MECP)-2 (ref. 16).

Overall, the functions of microglia in the healthy, diseased or injured brain are complex and diverse, and far from being understood. Consequently, there is an urgent need for genetic approaches to study these cells in their physiological setting; that is, the intact organism. Previous attempts to study microglial functions by genetic targeting *in vivo* largely failed owing to the lack of any specific microglial markers or genes that would allow researchers to genetically discriminate these cells from close relatives of the myeloid lineage[17]. Here we developed a genetic system for targeting microglia that involves expression of Cre recombinase driven by the *Cx3cr1* promoter and takes advantage of microglial longevity and concomitant self-renewal. Our approach takes into account that microglia migrate to the CNS during early embryogenesis and that there is no replacement of microglia from the circulation in adult animals[7].

Besides astrocytes, microglia are the main source and target of cytokines in the CNS[2]. Indeed, they can produce a plethora of molecules, such as tumor necrosis factor (TNF)-α, interleukin (IL)-1β, Fas ligand, interferon (IFN)-γ and chemokines such as CCL2, CCL3, CCL4, CCL5, CXCL9, CXCL10, but also anti-apoptotic molecules, many of which are targets of nuclear factor-κB (NF-κB) and its upstream kinases. One of these NF-κB–modulating molecules is TAK1, which belongs to the family of mitogen-activated protein kinase kinase kinases (MAP3Ks). TAK1 is usually activated by cytokines such as TNF-α, as well as by lipopolysaccharide (LPS) and TGF-β, and is involved in controlling the activation of p38 mitogen-activated protein kinase kinase (p38MAPKK), Jun N-terminal kinase (JNK) and

[1]Institute of Neuropathology, University of Freiburg, Freiburg, Germany. [2]Faculty of Biology, University of Freiburg, Freiburg, Germany. [3]Department of Immunology, The Weizmann Institute of Science, Rehovot, Israel. [4]Department of Internal Medicine III, University Hospital Rheinisch-Westfälische Technische Hochschule Aachen, Aachen, Germany. [5]Institute of Virology, Technische Universität München/Helmholtz Zentrum München, Munich, Germany. [6]BIOSS Centre for Biological Signalling Studies, University of Freiburg, Freiburg, Germany. [7]These authors contributed equally to this work. Correspondence should be addressed to M.P. (marco.prinz@uniklinik-freiburg.de) or S.J. (s.jung@weizmann.ac.il).

Received 14 May; accepted 5 September; published online 29 September 2013; doi:10.1038/nn.3531

NF-κB in various cellular systems[18]. Upon stimulation, TAK1 and its adaptors, TAB2, TAB3 and NEMO, are recruited to polyubiquitinated receptor (TNFSF)-interacting serine-threonine kinase 1 (RIPK1), thus allowing TAK1 to phosphorylate and activate the catalytic inhibitor of κB kinase (IKK) subunits[19]. Subsequent IKK activation induces the expression of many cytokines, chemokines and adhesion molecules that mediate the recruitment and activation of immune cells. In addition, TAK1 protects cells from cytokine-induced death by inducing the expression of antiapoptotic proteins[20]. Importantly, we have previously shown that TAK1 also exerts antinecrotic and anticarcinogenic features that ensure normal tissue homeostasis[21]. Thus, the net effect of TAK1 signaling in autoimmune demyelinating disease is probably determined by the balance between those opposing proinflammatory and antiapoptotic/antinecrotic activities, which may have distinct functions in specific CNS cell types. Although it has been demonstrated that TAK1 is essential for many innate and adaptive immune responses[22,23], its function in microglia during health and disease remains elusive. We therefore investigated this unresolved issue.

RESULTS

Cx3cr1^{Cre} mice: a new tool to study microglial function

Microglia show high expression of the chemokine receptor CX_3CR1 (ref. 24), which seems to be involved in the communication of these cells with selected neurons that express the corresponding CX_3CR1 ligand CX_3CL1 (fractalkine)[25,26]. Notably, CX_3CR1 is more broadly expressed—for example, on circulating monocytes, as well as subsets of peripheral mononuclear phagocytes, including macrophages and dendritic cells, and myeloid progenitors in the bone marrow[24,27]. To visualize expression of CX_3CR1, we previously generated CX_3CR1^{GFP} mice, which harbor a targeted replacement of a *Cx3cr1* allele with a cDNA encoding the enhanced green fluorescence protein (eGFP), which demonstrated that in the adult brain parenchyma only microglia express this marker[24].

To exploit *Cx3cr1* promoter activity for fate mapping, we recently replaced the *Cx3cr1* gene with sequences encoding either Cre recombinase (*Cx3cr1*^{Cre}) or a Cre recombinase fused to a mutant estrogen ligand-binding domain (*Cx3cr1*^{CreER})[28]. The latter requires the presence of the estrogen antagonist tamoxifen (TAM) for activation. Given the restricted expression of CX_3CR1 in the CNS parenchyma—namely, on microglia only—*Cx3cr1*^{Cre} and *Cx3cr1*^{CreER} mice should prove especially valuable for dissecting microglial function *in vivo*. To probe this potential, we compared these mice with existing models used for microglial targeting—namely, mice expressing Cre from the lysozyme (*LysM*, or *Lyz2*)[29] and integrin-α_X (*CD11c*, or *Itgax*)[30] loci—with respect to their microglial reporter gene activation pattern. To this end, all four lines were crossed to *ROSA26* (*R26*)-*yfp* reporter animals. We started by exploring the recombination efficacy in microglia in different CNS regions of *Cx3cr1*^{Cre}:*R26-yfp* animals (**Fig. 1a**). *Ex vivo*–isolated microglia from adult mice were gated by flow cytometry as a $CD45^{lo}CD11b^{+}$ cell population and the percentage of YFP^{+} cells was determined (**Fig. 1b**). Virtually all microglial cells (99.4 ± 0.1%) were labeled with YFP in the CNS.

To confirm these findings on a microscopic level, we examined parenchymal microglia histologically in several regions of the CNS,

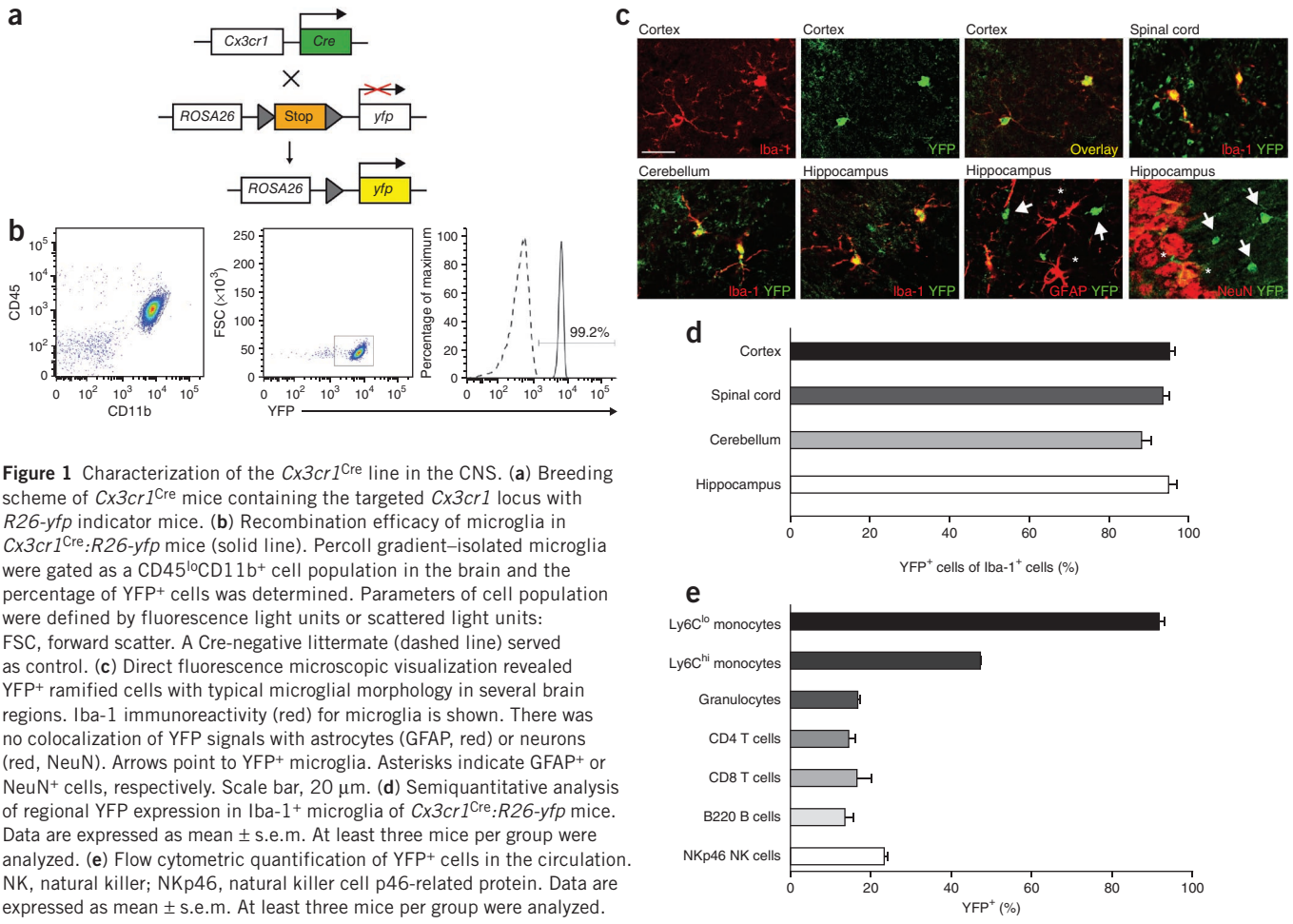

Figure 1 Characterization of the *Cx3cr1*^{Cre} line in the CNS. (**a**) Breeding scheme of *Cx3cr1*^{Cre} mice containing the targeted *Cx3cr1* locus with *R26-yfp* indicator mice. (**b**) Recombination efficacy of microglia in *Cx3cr1*^{Cre}:*R26-yfp* mice (solid line). Percoll gradient–isolated microglia were gated as a $CD45^{lo}CD11b^{+}$ cell population in the brain and the percentage of YFP^{+} cells was determined. Parameters of cell population were defined by fluorescence light units or scattered light units: FSC, forward scatter. A Cre-negative littermate (dashed line) served as control. (**c**) Direct fluorescence microscopic visualization revealed YFP^{+} ramified cells with typical microglial morphology in several brain regions. Iba-1 immunoreactivity (red) for microglia is shown. There was no colocalization of YFP signals with astrocytes (GFAP, red) or neurons (red, NeuN). Arrows point to YFP^{+} microglia. Asterisks indicate $GFAP^{+}$ or $NeuN^{+}$ cells, respectively. Scale bar, 20 μm. (**d**) Semiquantitative analysis of regional YFP expression in Iba-1^{+} microglia of *Cx3cr1*^{Cre}:*R26-yfp* mice. Data are expressed as mean ± s.e.m. At least three mice per group were analyzed. (**e**) Flow cytometric quantification of YFP^{+} cells in the circulation. NK, natural killer; NKp46, natural killer cell p46-related protein. Data are expressed as mean ± s.e.m. At least three mice per group were analyzed.

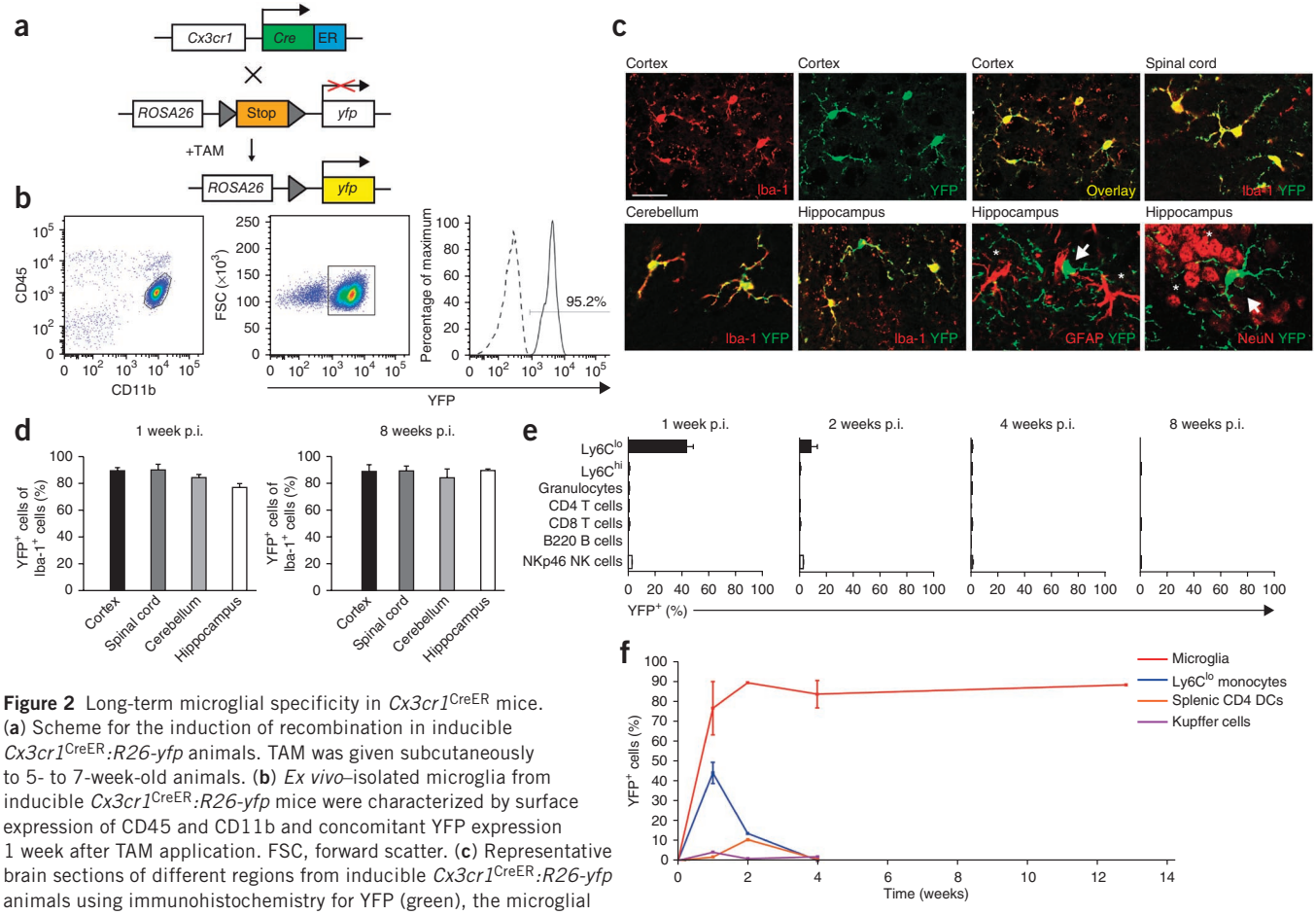

Figure 2 Long-term microglial specificity in *Cx3cr1*^{CreER} mice. (**a**) Scheme for the induction of recombination in inducible *Cx3cr1*^{CreER}*:R26-yfp* animals. TAM was given subcutaneously to 5- to 7-week-old animals. (**b**) *Ex vivo*–isolated microglia from inducible *Cx3cr1*^{CreER}*:R26-yfp* mice were characterized by surface expression of CD45 and CD11b and concomitant YFP expression 1 week after TAM application. FSC, forward scatter. (**c**) Representative brain sections of different regions from inducible *Cx3cr1*^{CreER}*:R26-yfp* animals using immunohistochemistry for YFP (green), the microglial marker Iba-1 (red), GFAP (red) or NeuN (red) 8 weeks after TAM injection. Arrows highlight YFP$^+$ microglia. Asterisks indicate GFAP$^+$ or NeuN$^+$ cells, respectively. Scale bar, 20 µm. (**d**) Semi-quantitative analysis of regional YFP expression in Iba-1$^+$ microglia in inducible *Cx3cr1*^{CreER}*:R26-yfp* mice at indicated time points post-induction (p.i.). Data are expressed as mean ± s.e.m. At least three mice per group were analyzed. (**e**) Kinetics of YFP$^+$ cells in the circulation by FACS. Data are expressed as mean ± s.e.m. Four mice were examined in each experimental group. NK, natural killer. (**f**) Induction but subsequent progressive loss of cells harboring gene rearrangements in peripheral myeloid cells (Ly6C^{lo} monocytes, splenic CD4$^+$ dendritic cells (DCs)) and tissue macrophages (Kupffer cells) but persistence of genomic modification in microglia. Data are expressed as mean ± s.e.m. At least three mice were examined in each experimental group.

including the neocortex, cerebellum, hippocampus and spinal cord (**Fig. 1c**). Microscopic investigation of these areas confirmed that the vast majority of Iba-1$^+$ cells with typical microglial morphology, such as a round to spindle-shaped soma and a distinct arborization pattern, expressed YFP. Assessment of at least 200 Iba-1$^+$ microglial cells per brain region on a single-cell level revealed a high YFP expression rate (>93%) in microglia in the cortex, hippocampus and spinal cord. In the cerebellum, 88.1 ± 2.4% of the parenchymal microglia were double-positive for Iba-1 and YFP (**Fig. 1d**). Of note, we were unable to detect any ectopic gene expression in non-Iba-1$^+$ cells in the CNS, as we found neither double-positive glial fibrillary acidic protein (GFAP)-expressing astrocytes nor NeuN$^+$ neurons in *Cx3cr1*^{Cre}*:R26-yfp* animals. Fluorescence-activated cell sorting (FACS) analysis of blood cells revealed YFP expression in Ly-6C^{lo} and Ly-6C^{hi} monocytes, mirroring the expression of the CX_3CR1 receptor in the circulation as described previously (**Fig. 1e**)[27]. In sum, microglial recombination is highly sufficient and specific in the CNS of *Cx3cr1*^{Cre}*:R26-yfp* animals, but it targets peripheral CX_3CR1^+ cells as well[27].

Once established in the CNS, microglia persist throughout the entire life of the organism without any appreciable input from circulating blood cells, owing to their longevity and their capacity of self-renewal[31,32]. We therefore sought to use this unique feature of microglia to distinguish this cell type from short-lived blood cells derived from the definitive hematopoiesis, such as monocytes, in order to specifically target microglia. For this purpose, we challenged *Cx3cr1*^{Cre}*:R26-yfp* animals, harboring the latent Cre recombinase[28], with TAM exposure at 5 to 7 weeks of age and determined microglial labeling at several time points after application (**Fig. 2a**). As in *Cx3cr1*^{CreER}*:R26-yfp* mice, FACS analysis demonstrated a high percentage (94.8 ± 0.2%) of YFP$^+$ cells among CD45^{lo}CD11b$^+$ microglia (**Fig. 2b**). Histological examination confirmed the FACS data and revealed a high percentage of Iba-1-labeled microglia in the cortex, spinal cord, cerebellum and hippocampus that coexpressed YFP (**Fig. 2c**). Quantitative examination on histological slices showed high reporter gene activation in all CNS regions both 1 and 8 weeks after TAM injection (**Fig. 2d**). These data confirm the earlier notion that brain microglia are a stable population that is not appreciably supplemented by blood cells within 8 weeks[31,32]. We found no ectopic YFP expression in astrocytes or neurons of *Cx3cr1*^{CreER}*:R26-yfp* mice. Notably, CX_3CR1^+ YFP-expressing blood cells such as monocytes are short-lived[28] and are therefore replaced by their YFP$^-$ monocyte progeny harboring unrearranged *R26-yfp* alleles.

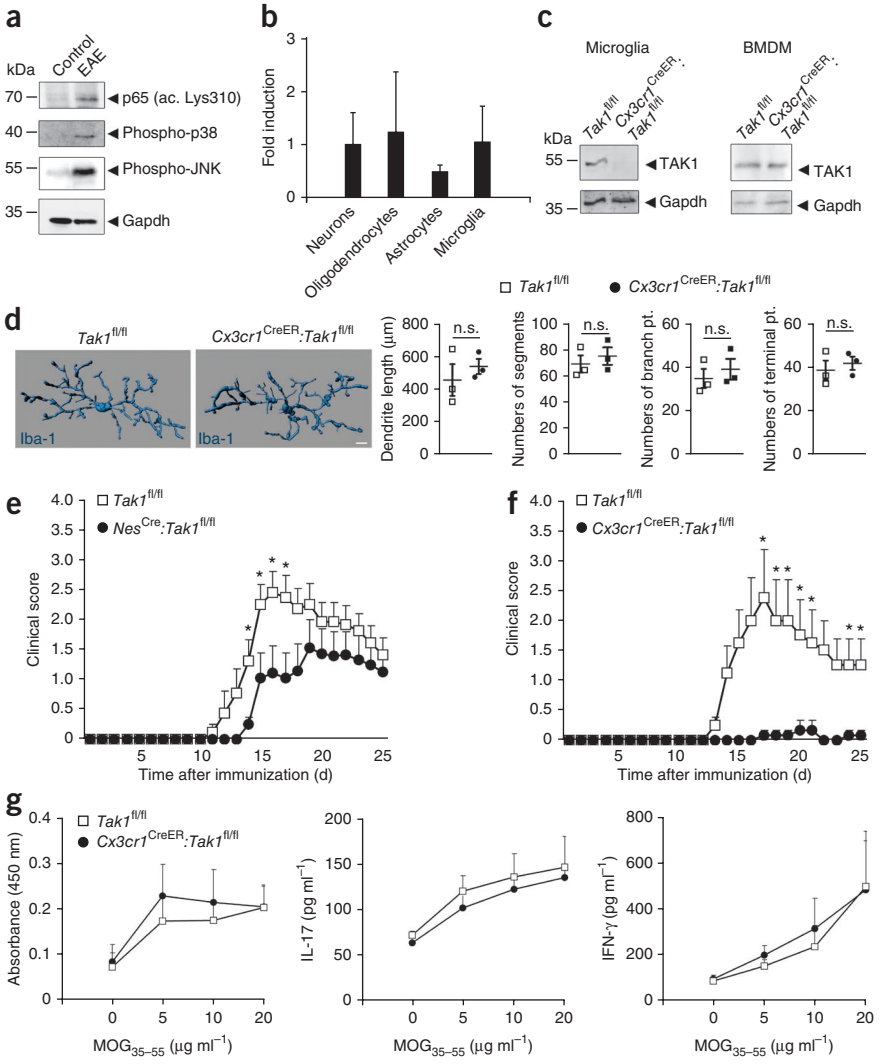

Figure 3 Microglia-restricted absence of TAK1 abolishes autoimmune inflammation in the CNS. (**a**) Immunoblot for activated NF-κBp65 (p65; acetylated (ac.) on Lys310), p38MAPKK (p38) and JNK on spinal cord lysates of diseased (EAE) or healthy (control) mice. Gapdh is shown as loading control. Full-length blot images are presented in **Supplementary Figure 10**. (**b**) Quantitative reverse transcription (RT)-PCR for *Tak1* in primary cells. Data are expressed as ratio of *Tak1* expression versus endogenous *Gapdh* relative to that in neurons and shown as mean ± s.e.m. (**c**) Immunoblot on *ex vivo*–isolated microglia or bone marrow–derived macrophages (BMDM) from *Cx3cr1*^{CreER}*:Tak1*$^{fl/fl}$ mice 4 weeks after TAM injection into 5- to 7-week-old animals. Gapdh is shown as loading control. Full-length blot images are presented in **Supplementary Figure 10**. (**d**) Morphology of microglia in the absence of TAK1 4 weeks after TAM injection. Left, Imaris (Bitplane)-based three-dimensional reconstruction of a representative Iba-1$^+$ microglial cell in a *Tak1*$^{fl/fl}$ and a *Cx3cr1*^{CreER}*:Tak1*$^{fl/fl}$ mouse, respectively. Scale bar, 10 µm. Right, Imaris-based automated quantification of microglial morphology. Data represent means ± s.e.m. of at least four cells in three animals per group; n.s., not significant. (**e**) EAE was induced by active immunization of *Nes*^{Cre}*:Tak1*$^{fl/fl}$ ($n = 6$) and *Tak1*$^{fl/fl}$ ($n = 6$) mice or (**f**) *Cx3cr1*^{CreER}*:Tak1*$^{fl/fl}$ ($n = 6$) and *Tak1*$^{fl/fl}$ ($n = 4$) animals and disease was scored (see Online Methods). Each data point represents the mean ± s.e.m. Asterisks indicate statistical significance determined by Mann-Whitney *U* test ($P \leq 0.05$). One representative experiment out of three with at least five mice per group is presented. (**g**) Recall assay in *Cx3cr1*^{CreER}*:Tak1*$^{fl/fl}$ mice. Lymph-node T cells were collected and cultured for 48 h at indicated $MOG_{35–55}$ concentrations. Proliferation was measured by BrdU incorporation for 16 h (left). Proliferation as determined by BrdU incorporation (left), IL-17 release (middle) and IFN-γ release (right) were measured by ELISA. IL-17 (middle) and IFN-γ (right) release were measured by ELISA. Data represent mean ± s.e.m. of at least three animals per group. Results are representative of two independent experiments.

In fact, 2 weeks after TAM application, we already observed very few YFP$^+$ blood cells (<2% of Ly-6C^{lo} monocytes), and these were virtually undetectable 4 weeks later (<0.2% of Ly-6C^{lo} monocytes) (**Fig. 2e**). Notably, gene recombination in microglia of *Cx3cr1*^{CreER} mice was high under different TAM administration routes (**Supplementary Fig. 1**) and remained stable over several weeks, whereas Ly6C^{lo} monocytes and splenic CD4$^+$ dendritic cells were no longer labeled (**Fig. 2f** and **Supplementary Fig. 2**). Due to the cellular kinetics of blood cell replenishment versus microglial longevity, *Cx3cr1*^{CreER}*:R26-yfp* animals thus present a new tool for targeting specifically microglia *in vivo*. Accordingly, we could easily distinguish YFP-labeled CD11b$^+$ microglia from YFP$^-$ infiltrating Ly6C^{lo} and Ly6C^{hi} monocytes after induction of experimental autoimmune encephalomyelitis (EAE) in *Cx3cr1*^{CreER}*:R26-yfp* animals (**Supplementary Fig. 3**).

Previous studies used the *LysM* promoter[29] or the *CD11c* promoter[30] to target microglia *in vivo*. We hence generated *LysM*^{Cre}*:R26-yfp* and *CD11c*^{Cre}*:R26-yfp* mice and examined microglia-specific gene activation in these strains (**Supplementary Figs. 4** and **5**). The frequently used *LysM*^{Cre} strain showed an average recombination rate in Iba-1$^+$ spinal cord microglia of 45.5 ± 2.5% YFP$^+$ cells in FACS analysis and 45.6 ± 5.3% as determined by histology (**Supplementary Fig. 4a**,**b**). Of note, circulating blood cells, especially granulocytes and monocytes, were also highly YFP-labeled (**Supplementary Fig. 4d**). In line with the absence of CD11c expression on resting microglia[32], *CD11c*^{Cre}*:R26-yfp* mice exhibited a low recombination efficacy in microglia with less than 7% of YFP$^+$CD45^{lo}CD11b$^+$ microglia as determined by FACS (**Supplementary Fig. 5a**). On individual brain sections, however, the percentage of positively labeled parenchymal microglia was even less in most examined brain regions (4.4 ± 0.5% in spinal cord, 5.2 ± 4.2% in cortex, 4.0 ± 2.4% in cerebellum, 15.8 ± 6.8% in hippocampus) (**Supplementary Fig. 5b**,**c**). In contrast to the poor gene activation in microglia, *CD11c*^{Cre}*:R26-yfp* mice displayed a high recombination in peripheral Ly-6C^{lo} monocytes and also lymphocytes (**Supplementary Fig. 5d**).

Taken together, the newly developed *Cx3cr1*^{Cre} line and especially the TAM-inducible *Cx3cr1*^{CreER} line provide a tool to selectively target microglia with high frequency and stable genetic modification over a prolonged period of time. Overall, these mouse lines are superior to the Cre lines used so far to study microglia *in vivo*. To be targeted by this system, cells must express CX_3CR1 at the time of TAM

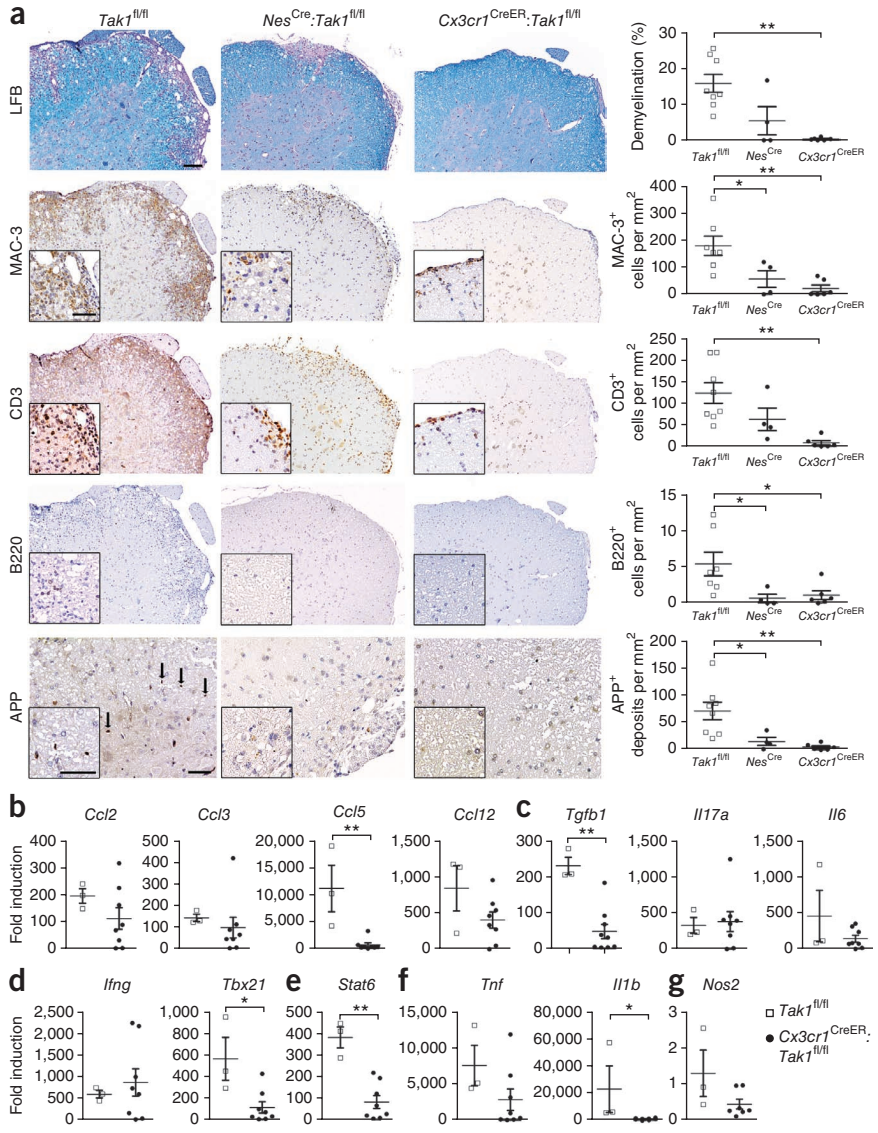

Figure 4 Reduced CNS damage and immune suppression in *Cx3cr1*^{CreER}*:Tak1*$^{fl/fl}$ mice. (**a**) Left, histology of spinal cord sections using Luxol fast blue (LFB) for demyelination, MAC-3 for macrophages, CD3 for T lymphocytes, B220 for B cells and amyloid precursor protein (APP) for axonal damage. Scale bars, 100 µm (main panels, top four rows), 50 µm (main panels, APP) and 50 µm (insets; MAC-3 bar applies to CD3 and B220 also). Right, quantification of demyelination, cell infiltrates and axonal damage. Each symbol indicates the mean of one mouse. Significant differences of *Tak1*$^{fl/fl}$ to *Nes*^{Cre}*:Tak1*$^{fl/fl}$ or *Cx3cr1*^{CreER}*:Tak1*$^{fl/fl}$ are determined by Mann-Whitney *U* test (Mac-3: *Nes*^{Cre}*:Tak1*$^{fl/fl}$, *Cx3cr1*^{CreER}*:Tak1*$^{fl/fl}$; CD3: *Cx3cr1*^{CreER}*:Tak1*$^{fl/fl}$; B220: *Nes*^{Cre}*:Tak1*$^{fl/fl}$) or unpaired *t*-test (LFB: *Cx3cr1*^{CreER}*:Tak1*$^{fl/fl}$; B220: *Cx3cr1*^{CreER}*:Tak1*$^{fl/fl}$, APP: *Nes*^{Cre}*:Tak1*$^{fl/fl}$, *Cx3cr1*^{CreER}*:Tak1*$^{fl/fl}$) and marked with asterisks (*$P < 0.05$, **$P < 0.01$). (**b**–**g**) Gene expression levels for chemokines (**b**) and TH17- (**c**), TH1- (**d**) and TH2 (**e**)-linked factors, as well as proinflammatory cytokines (**f**) and *Nos2* (**g**) in the spinal cord of *Tak1*$^{fl/fl}$ or *Cx3cr1*^{CreER}*:Tak1*$^{fl/fl}$ mice. Each symbol represents one mouse. Data are expressed as the ratio of induced factors normalized to endogenous *Gapdh* compared with healthy controls (except for **g**, which is normalized to *Tak1*$^{fl/fl}$) and expressed as mean ± s.e.m. Significant differences are determined by Mann-Whitney *U* test (*Ccl5*, *Tbx21*) or unpaired *t*-test (*Tgfb1*, *Stat6*, *Il1b*) and marked with asterisks (*$P < 0.05$, **$P < 0.01$).

application and be self-maintaining. Liver Kupffer cells, for instance, do not meet the first requirement, while intestinal macrophages have a limited half-life of 3 weeks[28].

Microglia-specific TAK1 is key in autoimmune demyelination

To investigate which cellular activation pathways are induced upon CNS inflammation, we analyzed spinal cord homogenates from animals with EAE, a widely accepted mouse model for multiple sclerosis, by western blotting. We observed a profound activation of the signaling molecules p38MAPKK, JNK and NF-κB subunit p65 (**Fig. 3a**). Notably, all these signaling cascades are controlled by a single kinase, TAK1 (ref. 18). Quantitative expression analysis of *Tak1* (*Map3k7*) mRNA revealed comparable expression in primary neuroectodermal cells, such as neurons and astrocytes, as well as mesodermal microglia *in vitro* (**Fig. 3b**). To investigate the involvement of TAK1 in distinct categories of brain resident cells in autoimmune diseases, we examined EAE development in mice lacking TAK1 in either neuroectodermal cells or microglia only. Mice carrying *loxP*-flanked ('floxed'; fl) *Tak1* alleles were crossed with mice expressing Cre from the nestin locus (*Nes*^{Cre} mice) or with *Cx3cr1*^{CreER} mice. The *Nes*^{Cre} transgene mediates excision of *loxP*-flanked sequences in early neural precursors during embryonic life, resulting in efficient target gene inactivation in all neuroectodermal cells of the CNS, including neurons, astrocytes and oligodendrocytes, but sparing microglia[33,34].

Nes^{Cre}*:Tak1*$^{fl/fl}$ mice were born at normal Mendelian frequencies and did not show any overt abnormalities. Immunoblot analysis 4 weeks after TAM injection in *Cx3cr1*^{CreER}*:Tak1*$^{fl/fl}$ mice confirmed efficient ablation of TAK1 on a protein level from *ex vivo*–isolated microglia (as progeny of the primitive hematopoiesis), but not from bone marrow–derived macrophages (as part of the definitive hematopoiesis) (**Fig. 3c**). Mice with induced microglia-specific TAK1 deficiency were viable and did not demonstrate apparent abnormalities. Because TAK1 has been described as vital for the development and homeostasis of distinct myeloid cell subsets in the periphery, we rigorously examined steady-state microglial features in *Cx3cr1*^{CreER}*:Tak1*$^{fl/fl}$ animals. We first performed a detailed, quantitative morphometric analysis of Iba-1^{+} microglia lacking TAK1 (**Fig. 3d**). TAK1-deficient microglia showed typical resting, unactivated morphology, such as round to spindle-shaped somata and a distinct arborization pattern with finely delineated processes, as demonstrated in three-dimensional reconstructions of confocal *z*-stacks. Cell dimensions, as judged by total dendrite length (*Tak1*$^{fl/fl}$, 460.7 ± 96.2 µm (mean ± s.e.m.); *Cx3cr1*^{CreER}*:Tak1*$^{fl/fl}$, 543.0 ± 45.6 µm; $P = 0.36$), the number of dendrite segments (*Tak1*$^{fl/fl}$, 69.4 ± 6.6; *Cx3cr1*^{CreER}*:Tak1*$^{fl/fl}$, 75.4 ± 6.7; $P = 0.99$), the number of dendrite branch points (*Tak1*$^{fl/fl}$, 35.0 ± 4.2; *Cx3cr1*^{CreER}*:Tak1*$^{fl/fl}$, 39.1 ± 4.6; $P = 0.91$) and the number of dendrite terminal points (*Tak1*$^{fl/fl}$, 39.0 ± 4.3; *Cx3cr1*^{CreER}*:Tak1*$^{fl/fl}$,

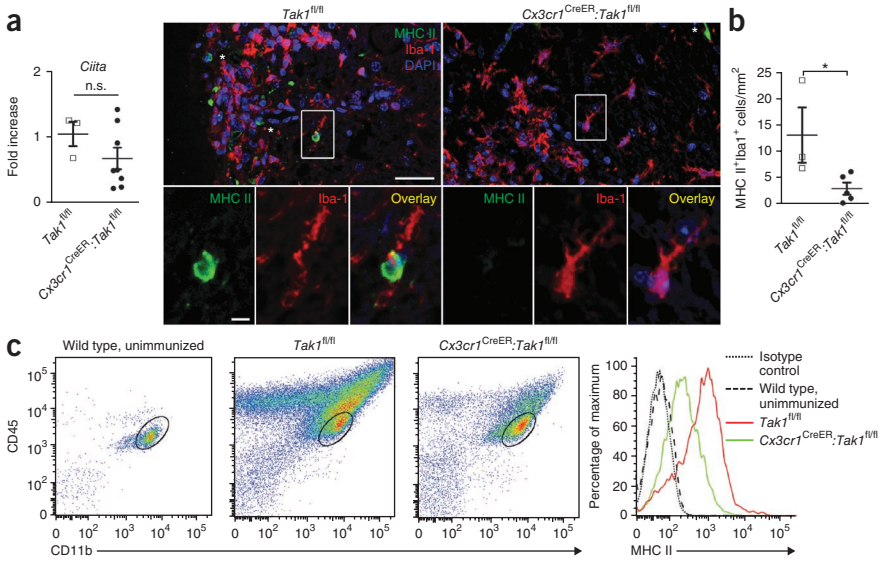

Figure 5 Diminished MHC class II expression in *Cx3cr1*^{CreER}*:Tak1*$^{fl/fl}$ mice during EAE. (**a**) Quantitative RT-PCR analysis of *Ciita* mRNA from spinal cord samples of *Tak1*$^{fl/fl}$ or *Cx3cr1*^{CreER}*:Tak1*$^{fl/fl}$ mice. Each symbol represents one mouse. Data are expressed as the ratio of induced factors normalized to endogenous *Gapdh* compared with healthy controls and expressed as mean ± s.e.m. $P = 0.23$; n.s., not significant. (**b**) Left, immunofluorescence images of MHC class II expression (green) on Iba-1$^+$ (red) microglia or macrophages (cell highlighted with a white frame is enlarged below) and on Iba-1$^-$ cells (asterisks) in the parenchyma of EAE-affected *Tak1*$^{fl/fl}$ and *Cx3cr1*^{CreER}*:Tak1*$^{fl/fl}$ mice. Nuclei are stained with 4,6-diamidino-2-phenylindole (DAPI; blue). Scale bars, 10 µm (top) and 5 µm (bottom). Right, quantification. Each symbol indicates the mean of one mouse. Significant difference is determined by unpaired *t*-test (*$P < 0.049$). (**c**) Flow cytometric quantification of MHC class II expression on CD11b$^+$CD45^{lo} microglia during EAE. Left, a representative dot plot for each condition from one of two independent experiments. Right, EAE diseased *Tak1*$^{fl/fl}$ mice, red; *Cx3cr1*^{CreER}*:Tak1*$^{fl/fl}$ mice, green. Healthy unimmunized animals (dashed line) and isotype antibody (dotted line) served as controls.

41.9 ± 2.9; $P = 0.63$) were unaltered in TAK1-deficient microglia. Further histological analysis of brain sections of these mice did not reveal any gross morphological defects, microgliosis or astrogliosis, suggesting that expression of TAK1 in microglia is not essential for proper tissue homeostasis in the adult brain (**Supplementary Fig. 6**). In addition, absence of TAK1 in microglia did not alter major histocompatibility complex (MHC) class II or Lamp-2 expression (as a marker of phagocytosis) in these cells (**Supplementary Fig. 7**).

To compare microglia- and neuroectoderm-specific function of TAK1 in the pathogenesis of EAE, we immunized *Nes*^{Cre}*:Tak1*$^{fl/fl}$ and *Cx3cr1*^{CreER}*:Tak1*$^{fl/fl}$ mice and their littermate controls with myelin oligodendrocyte glycoprotein $(MOG)_{35–55}$ peptide and monitored disease progression by clinical assessment. Control littermates carrying the respective floxed *Tak1* alleles but lacking expression of the Cre recombinase exhibited a typical disease course, developing signs of paralysis. In contrast, while *Nes*^{Cre}*:Tak1*$^{fl/fl}$ mice had a similar disease onset, they developed a slightly milder disease showing fewer clinical symptoms (**Fig. 3e**). Notably, *Cx3cr1*^{CreER}*:Tak1*$^{fl/fl}$ animals were highly resistant to $MOG_{35–55}$ immunization, which resulted in a considerably less severe disease (**Fig. 3f**). These results indicate that microglia-specific rather than neuroectodermal expression of TAK1 is essential for the pathogenesis of autoimmune inflammation of the CNS.

The efficient activation of T lymphocytes is a critical requirement for the induction of CNS inflammation and pathology in EAE. As we have used microglia-specific ablation of TAK1 in our studies, peripheral immune functions should not be affected in these mice. To directly address this point, we examined the generation of $MOG_{35–55}$-specific T cells in TAM-treated *Cx3cr1*^{CreER}*:Tak1*$^{fl/fl}$ animals. We isolated lymphocytes from immunized mice and tested *in vitro* recall response upon secondary exposure to $MOG_{35–55}$ peptide (**Fig. 3g**). T cells derived from *Cx3cr1*^{CreER}*:Tak1*$^{fl/fl}$ mice did not show impaired recall response to the $MOG_{35–55}$ compared to that of control littermates, as assessed by measurement of proliferation and the production of IL-17 and IFN-γ. This suggests that the ameliorated EAE of the animals harboring TAK1-deficient microglia is not caused by impaired peripheral T cell responses.

To investigate the reason underlying the improved clinical outcome, we examined spinal cord sections of *Nes*^{Cre}*:Tak1*$^{fl/fl}$ and *Cx3cr1*^{CreER}*:Tak1*$^{fl/fl}$ mice and their respective control littermates by immunohistochemistry 25 d after immunization (**Fig. 4a**). In control mice, we detected many MAC3$^+$ macrophages as well as many CD3$^+$ T cells and B220$^+$ B cells in the meninges and in the spinal cord parenchyma. These cellular infiltrates were accompanied by histological signs of severe demyelination in the white matter, as demonstrated by Luxol fast blue staining, as well as axonal damage, as visualized by immunohistochemical staining for amyloid precursor protein. In comparison, *Nes*^{Cre}*:Tak1*$^{fl/fl}$ mice had fewer inflammatory cells, the myelin remained more intact and we detected only a few minor signs of axonal damage. However, analysis of *Cx3cr1*^{CreER}*:Tak1*$^{fl/fl}$ animals revealed minimal amounts of immune cell infiltration in the spinal cord and only subtle signs of myelin destruction and axonal loss, findings that mirrored the much ameliorated clinical course of EAE exhibited by these animals. These results demonstrate that loss of TAK1 mainly in mesodermal microglia and, to a lesser extent, in neuroectodermal cells protects mice from EAE, potentially by affecting the influx of peripheral immune cells into the CNS.

We next quantified the expression of chemokines (**Fig. 4b**); T helper cell (TH)-17- (**Fig. 4c**), TH1- (**Fig. 4d**) and TH2-linked factors (**Fig. 4e**); and microglial effector molecules, such as *Tnf*, *Il1b* (**Fig. 4f**) and *Nos2* (**Fig. 4g**) in the CNS of immunized *Cx3cr1*^{CreER}*:Tak1*$^{fl/fl}$ mice. Whereas most genes showed a trend toward reduced expression as compared to that in controls, some TH1-, TH2- and TH17-related factors and effector molecules were significantly decreased. Therefore, the reduced EAE in the absence of TAK1 specifically in microglia seems linked to an overall dampened inflammatory immune response, rather than to a shift in the T effector cell profile. Because upregulation of MHC class II molecules is a sign of microglial activation during CNS inflammation[35], we investigated the expression of MHC class II in the CNS of immunized *Cx3cr1*^{CreER}*:Tak1*$^{fl/fl}$ mice (**Fig. 5**). Expression of *Ciita* mRNA, encoding a transactivator of MHC class II, was only slightly reduced in whole spinal cord homogenates in the absence of TAK1 (**Fig. 5a**), whereas significantly fewer MHC class II$^+$Iba-1$^+$ microglia or macrophages were detectable in *Cx3cr1*^{CreER}*:Tak1*$^{fl/fl}$ mice compared to *Tak1*$^{fl/fl}$ littermates (**Fig. 5b**). Notably, FACS analysis revealed lower MHC class II levels on the surface of CD11b$^+$CD45^{lo} microglia lacking TAK1 (**Fig. 5c**).

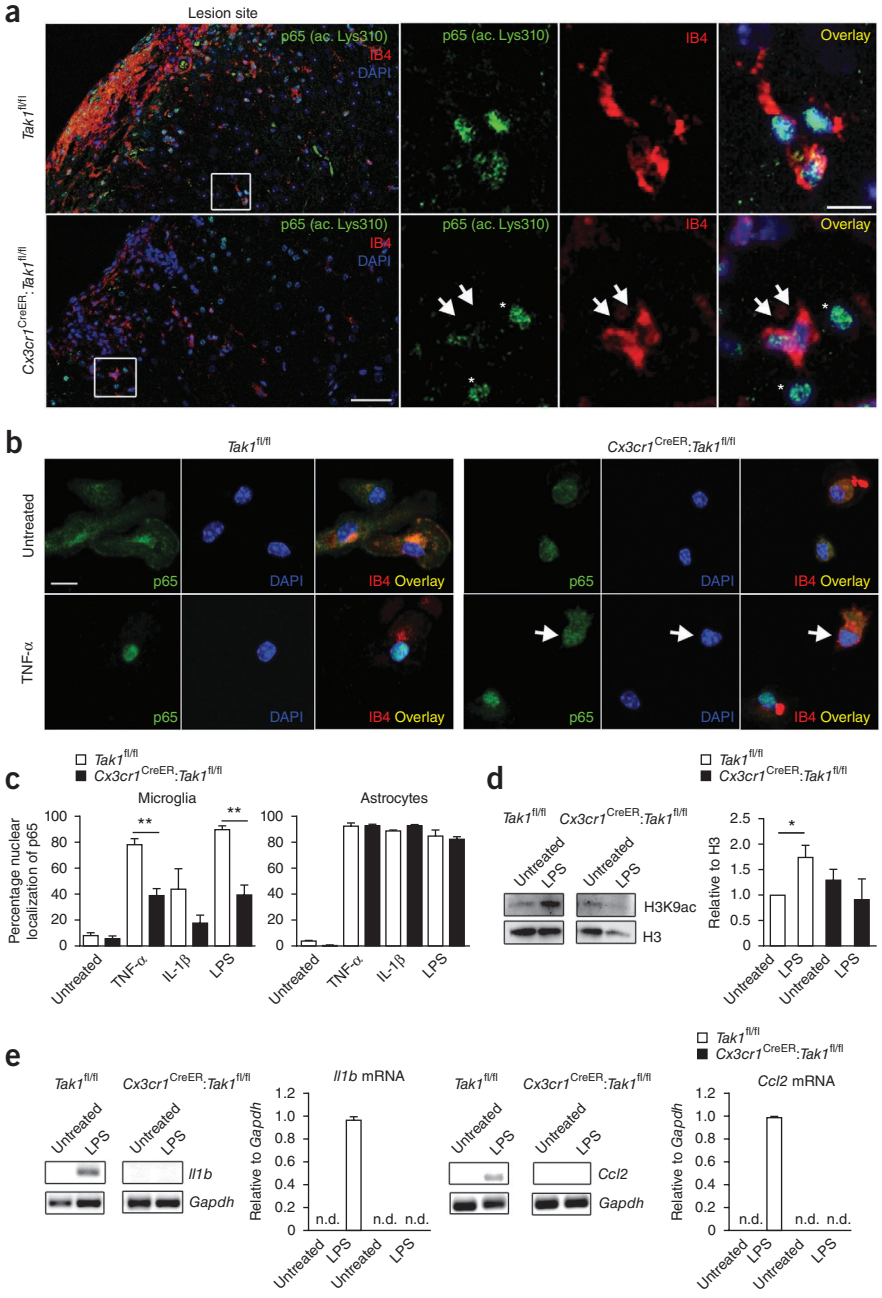

Figure 6 Microglia-specific TAK1 controls cell-intrinsic activation of NF-κBp65. (**a**) Nuclear NF-κBp65 localization (p65 ac. Lys310, green) is strongly induced in isolectin B4 (IB4)-positive microglia (red) in the spinal cord of *Tak1*$^{fl/fl}$ animals upon acute demyelination *in vivo* (top). In contrast, microglia of *Cx3cr1*^{CreER}:*Tak1*$^{fl/fl}$ mice were largely devoid of nuclear NF-κBp65 activation (bottom). Nuclei are stained with DAPI (4,6-diamidino-2-phenylindole; blue). Overview is shown at left (scale bar, 25 μm) and detail views at right (scale bar, 10 μm). Arrows highlight microglia without activated NF-κBp65. Asterisks indicate hematopoietic cells with activated NF-κBp65. Ac., acetylated. (**b**,**c**) Impaired NF-κBp65 translocation in primary microglia (**b**), but normal p65 activation in astrocytes (**c**) of *Cx3cr1*^{CreER}:*Tak1*$^{fl/fl}$ mice. Cells were left unstimulated (untreated) or were stimulated for 30 min with TNF-α, 120 min with IL-1β or 120 min with LPS then stained with p65 (green), IB4 (red) and DAPI (blue, **b**; scale bar, 10 μm), followed by quantification of cells showing p65 nuclear translocation (**c**). Data represent mean ± s.e.m. Significant differences are determined by unpaired *t*-test and marked with asterisks (**$P < 0.01$: for TNF-α, $P = 0.005$; for LPS, $P = 0.0001$). (**d**) Immunoblot depicting decreased H3K9ac in TAK1-deficient microglia challenged with LPS for 120 min. Bars represent mean ± s.e.m. of three independent experiments. Significant differences are determined by unpaired *t*-test and marked with an asterisk (*$P = 0.03$). Full-length blot images are presented in **Supplementary Figure 10**. Data are expressed as a ratio of H3K9ac normalized to H3. (**e**) RT-PCR of *Il1b* and *Ccl2* mRNA from primary microglia unstimulated (control, untreated) or stimulated with LPS for 120 min. Data are expressed as the ratio of induced factors normalized to endogenous *Gapdh*. Data represent mean ± s.e.m. Results are representative of three independent experiments. n.d., not detectable. Full-length gels images are presented in **Supplementary Figure 11**.

Taken together, our data demonstrate that the main mechanisms by which autoimmune demyelination in the CNS is induced are microglia-specific, TAK1-mediated cytokine and chemokine production and the regulation of antigen-presenting molecules that then allow the influx of inflammatory mononuclear cells, leading to subsequent destruction of axons and the loss of myelin.

TAK1 loss blocks microglial p65, JNK, ERK1/2 and p38MAPKK

TAK1 is considered a critical regulator of stress responses, immunity and inflammation that are mainly mediated by the downstream pathways p38MAPKK, JNK, extracellular signal–regulated kinases (ERK)-1 and ERK2, and NF-κBp65. To test whether microglia-restricted TAK1 ablation affects activation of the subsequent pathways *in vivo*, we performed immunohistochemistry with anti-acetylated NF-κBp65 (**Fig. 6a**) and antibodies to phosphorylated forms of ERK1/2, p38MAPKK and JNK (**Supplementary Fig. 8**). Double stainings for isolectin B4, a widely used marker for microglia, showed expression of p65 (acetylated), phospho-ERK1/2, phospho-p38MAPKK and phospho-JNK in reactive microglia in *Tak1*$^{fl/fl}$ animals that was abolished in microglia from *Cx3cr1*^{CreER}:*Tak1*$^{fl/fl}$ mice. These data suggest that TAK1-dependent ERK1/2, p38, JNK and NF-κB activation in microglia is essential for inflammatory gene expression in microglia during EAE. As proinflammatory and T helper–related gene expression has been shown to be important for the induction of EAE pathology, failure of TAK1-deficient microglia to upregulate TAK1-dependent pathways may explain the protection of *Cx3cr1*^{CreER}:*Tak1*$^{fl/fl}$ mice from EAE.

To further investigate the consequences of TAK1 deletion in microglia, we prepared primary microglial cell cultures from *Cx3cr1*^{CreER}:*Tak1*$^{fl/fl}$ and control mice and challenged these cultures with hydroxytamoxifen. Hydroxytamoxifen application resulted in >96% of the CD45^{+}CD11b^{+} cells being positive for YFP by flow cytometry, which was further corroborated by immunocytochemistry (**Supplementary Fig. 9**). To confirm that microglia from *Cx3cr1*^{CreER}:*Tak1*$^{fl/fl}$ mice showed impaired NF-κBp65 activation,

we measured NF-κB activity upon stimulation. Cells from control mice showed strong NF-κB activation in response to TNF-α, IL-1β or LPS, as shown by nuclear translocation of p65 (**Fig. 6b**,**c**). In contrast, microglia from *Cx3cr1*^{CreER}:*Tak1*$^{fl/fl}$ mice failed to fully activate NF-κBp65, suggesting efficient TAK1 deletion in the cultured microglia. As expected, astrocytes from both *Tak1*$^{fl/fl}$ and *Cx3cr1*^{CreER}:*Tak1*$^{fl/fl}$ mice showed similar NF-κBp65 activation. To obtain more mechanistic insights into the epigenetic regulation of gene expression in the absence of TAK1, we examined an epigenetic mark, acetylation of histone H3 on Lys9 (H3K9ac), that is associated with NF-κB activation[36] (**Fig. 6d**). Notably, upon LPS challenge, microglia from *Cx3cr1*^{CreER}:*Tak1*$^{fl/fl}$ mice lacked the NF-κB–induced increase of H3K9ac levels seen in wild-type controls. As a consequence, TAK1-deficient microglia, in contrast to wild-type cells, failed to induce NF-κB target genes *Il1b* and *Ccl2* (**Fig. 6e**), demonstrating that TAK1-dependent NF-κB activation is essential for microglial induction of proinflammatory mediators by microglia. Taken together, these results suggest that TAK1 deletion specifically in microglia leads to attenuated EAE pathology by inhibiting cell-autonomous activation of p38MAPKK, JNK and NF-κBp65, leading to subsequent suppression of proinflammatory genes and effector molecules in microglia.

DISCUSSION

Here we analyzed the *in vivo* function of TAK1 by using a new microglia-specific genetic approach, which helped define the role of this molecule during CNS autoimmunity in a cell-specific and inducible fashion. Our experimental approach allowed, to our knowledge for the first time, the *in vivo* delineation of the specific contribution of neuroectodermally derived (astrocyte, oligodendrocyte and neuron) versus mesodermally derived (microglia) CNS cell types to this pathogenic proinflammatory function. Although astrocyte-specific immune responses have been shown to be important in demyelinating mouse models *in vivo*[33,34], our results indicate that activation of microglia contributes to this pathology to a large extent as well. Infiltrating monocyte-derived macrophages, which can also be important in EAE pathogenesis[37], were not targeted by our genetic approach. Thus, *Cx3cr1*^{CreER} mice can also help to discriminate microglial effects from those attributed to disease-associated peripheral macrophages and monocytes recruited from the blood in the future.

We were able to demonstrate that microglia-endogenous TAK1 is a key regulator of CNS inflammation whose absence is associated with strongly diminished CNS inflammation and subsequent decreased tissue damage despite unaffected induction of encephalitogenic T cells in secondary lymphoid organs. Thus, we identify TAK1 as a new therapeutic target in autoimmune demyelination and establish the *Cx3cr1*^{CreER} system as a new genetic tool for dissecting microglia-specific functions *in vivo*.

Our findings suggest that the mechanism through which the inhibition of TAK1 in the CNS mediates its protective effects is by preventing the expression of proinflammatory mediators and effector molecules on the part of microglia. Activation of the adaptive immune system and the induction of myelin-specific auto-aggressive T cells is an obligatory requirement for the induction of EAE. However, the innate immune system is proposed to be important in autoimmune CNS inflammation by providing a permissive cytokine microenvironment that potentiates the immune response locally in the CNS[2].

Despite being the main source of proinflammatory molecules during EAE, microglia might influence autoimmune CNS inflammation by other mechanisms as well. An alternative mechanism through which microglia might regulate T cell responses in the CNS is by inducing T cell apoptosis through the expression of CD95 ligand or the proapoptotic molecule TRAIL[7]. It remains to be determined whether microglia-mediated is altered in *Cx3cr1*^{CreER}:*Tak1*$^{fl/fl}$ animals and whether this mechanism is relevant for disease amelioration in this model. Moreover, microglia-mediated damage in EAE might also be induced by the production of nitric oxide and its adducts, which disrupt CNS tissue integrity[8]. However, although mRNA levels of *Nos2* in the spinal cords of *Cx3cr1*^{CreER}:*Tak1*$^{fl/fl}$ mice were reduced compared to those in *Tak1*$^{fl/fl}$ mice, this difference did not reach statistical significance. Finally, reactivation of myelin-specific T cells within the CNS upon recognition of local autoantigens is thought to be critical for sustaining EAE[38]. But it is still under debate whether microglia present myelin-associated antigens to autoreactive T cells *in vivo*. One study claims that antigen-presenting capacity of microglia is not essential for promoting encephalitogenic T cells *in vitro*[39], whereas others consider presentation of myelin-associated antigens by microglia to be critical[35,40]. As we observed strongly reduced *Ciita* expression in the inflamed CNS of microglia-specific *Cx3cr1*^{CreER}:*Tak1*$^{fl/fl}$ mice, abrogated microglia-specific antigen presentation may also account for disease protection in these animals. However, the question whether there is a differential outcome when antigen is presented by microglia or other APCs remains to be resolved.

Although TAK1 inhibition does not obviously alter features of microglia in the normal brain, TAK1 has been shown to be vital for the function of other myeloid cells outside of the brain[18]. Deficiency of TAK1 in dendritic cells, for example, causes several defects in the immune system homeostasis, especially a deletion of dendritic cell subsets in lymphoid and nonlymphoid tissues as a result of marked apoptosis[41]. In dendritic cells, prosurvival signals from Toll-like receptors (TLRs), CD40 and receptor activator of NF-κB (RANK) are integrated by TAK1. Moreover, TAK1 regulates NKG2D receptor–mediated cytotoxicity of natural killer cells via the BCL10-MALT complex[42]. In neutrophils, by contrast, TAK1 negatively regulates p38MAPK activation[43], and, in normal hepatocytes under steady state conditions, it suppresses the *de novo* induction of inflammation, fibrosis and cancer in the liver by inhibiting procarcinogenic and pronecrotic pathways in a NEMO-dependent manner[21]. Therefore, even though microglial TAK1 is now an attractive molecular target for the treatment of autoimmune inflammation in the CNS, undesirable side effects that might influence the functions of other immune compartments in the body must be considered. As the net effect of TAK1 deletion in microglia is protective rather than disease-enhancing in EAE, strategies targeting TAK1 specifically in the CNS might prove useful for the treatment of multiple sclerosis without altering the peripheral immune responses, thus preventing unwanted immune effects.

Several transgenic mouse models have been generated in the past to target microglia *in vivo*[17].These models use different promoters, including the human lysozyme promoter (*LYZ*)[29], the MHC class I promoter H-2K^{b} (*H2-K1*) together with an immunoglobulin enhancer[44], the *Csf1r* promoter[45], the macrophage scavenger receptor type A promoter (*Msr1*)[46] and the *CD11c* promoter[47]. Until now, there were no transgenic lines available that could specifically target microglia while excluding other myeloid cell types. Indeed, dendritic cells and the CD11c^{+} subset of microglia were both ablated in a transgenic line carrying the diphtheria toxin receptor under the control of the *CD11c* promoter[47] (S.J., unpublished data). Similarly, a transgenic mouse model expressing HSV-TK under the control of the integrin-α_M (*CD11b*, or *Itgam*) promoter ablated not only proliferating microglia upon gancyclovir application but also CD11b^{+} bone marrow cells, inducing hemorrhagic death in these animals[9]. By taking advantage of unique features of microglia, such as their constitutively high expression

of CX3CR1 and their longevity, which distinguishes these cells from their peripheral blood counterparts, we here present, with the inducible *Cx3cr1*^{CreER} line, an *in vivo* model that allows the investigation of microglia-specific genes during health and disease at defined time points. This instrument may open new avenues in our understanding of the biology of microglia inside the most complex and enigmatic organ in mammals, the brain.

METHODS

Methods and any associated references are available in the online version of the paper.

Note: Any Supplementary Information and Source Data files are available in the online version of the paper.

ACKNOWLEDGMENTS

We thank M. Oberle, C. Fix and S. Gaupp for excellent technical assistance. Special thanks to M. Olschewski for help with the thorough statistical analysis of our data. M.P. was supported by the Bundesministerium für Bildung und Forschung–funded competence network of multiple sclerosis (KKNMS), the competence network of neurodegenerative disorders (KNDD), the Deutsche Forschungsgemeinschaft (SFB 992, FOR1336, PR 577/8-1), the Fritz-Thyssen Foundation, the Gemeinnützige Hertie Foundation (GHST) and Biogen Idec. P.F.M. was supported by an MD educational grant of the SFB620. M.H. was funded by the Helmholtz Foundation, the SFB-TR36, a European Research Council starting grant and the Helmholtz Alliance Preclinical Comprehensive Cancer Center. S.J. was supported by the Deutsche Forschungsgemeinschaft (FOR1336) and by the Israel Science Foundation.

AUTHOR CONTRIBUTIONS

T.G., P.W., P.F.M., S.M.B., K.K., D.V., Y.W., O.S. and M.D. conducted experiments. S.Y. generated the transgenic mice. S.J., M.H. and T.L. contributed to the *in vivo* studies and provided mice or reagents. M.P. and S.J. supervised the project and wrote the manuscript.

COMPETING FINANCIAL INTERESTS

The authors declare no competing financial interests.

1. Ransohoff, R.M. & Perry, V.H. Microglial physiology: unique stimuli, specialized responses. *Annu. Rev. Immunol.* **27**, 119–145 (2009).
2. Hanisch, U.K. Microglia as a source and target of cytokines. *Glia* **40**, 140–155 (2002).
3. Ginhoux, F. *et al.* Fate mapping analysis reveals that adult microglia derive from primitive macrophages. *Science* **330**, 841–845 (2010).
4. Schulz, C. *et al.* A lineage of myeloid cells independent of Myb and hematopoietic stem cells. *Science* **336**, 86–90 (2012).
5. Prinz, M. & Mildner, A. Microglia in the CNS: immigrants from another world. *Glia* **59**, 177–187 (2011).
6. Kierdorf, K. *et al.* Microglia emerge from erythromyeloid precursors via Pu.1- and Irf8-dependent pathways. *Nat. Neurosci.* **16**, 273–280 (2013).
7. Ransohoff, R.M. & Cardona, A.E. The myeloid cells of the central nervous system parenchyma. *Nature* **468**, 253–262 (2010).
8. Steinman, L., Martin, R., Bernard, C., Conlon, P. & Oksenberg, J.R. Multiple sclerosis: deeper understanding of its pathogenesis reveals new targets for therapy. *Annu. Rev. Neurosci.* **25**, 491–505 (2002).
9. Heppner, F.L. *et al.* Experimental autoimmune encephalomyelitis repressed by microglial paralysis. *Nat. Med.* **11**, 146–152 (2005).
10. Becher, B., Durell, B.G., Miga, A.V., Hickey, W.F. & Noelle, R.J. The clinical course of experimental autoimmune encephalomyelitis and inflammation is controlled by the expression of CD40 within the central nervous system. *J. Exp. Med.* **193**, 967–974 (2001).
11. Schwartz, M. & Moalem, G. Beneficial immune activity after CNS injury: prospects for vaccination. *J. Neuroimmunol.* **113**, 185–192 (2001).
12. Kerschensteiner, M., Stadelmann, C., Dechant, G., Wekerle, H. & Hohlfeld, R. Neurotrophic cross-talk between the nervous and immune systems: implications for neurological diseases. *Ann. Neurol.* **53**, 292–304 (2003).
13. Tremblay, M.È., Lowery, R.L. & Majewska, A.K. Microglial interactions with synapses are modulated by visual experience. *PLoS Biol.* **8**, e1000527 (2010).
14. Paolicelli, R.C. *et al.* Synaptic pruning by microglia is necessary for normal brain development. *Science* **333**, 1456–1458 (2011).
15. Marín-Teva, J.L. *et al.* Microglia promote the death of developing Purkinje cells. *Neuron* **41**, 535–547 (2004).
16. Derecki, N.C. *et al.* Wild-type microglia arrest pathology in a mouse model of Rett syndrome. *Nature* **484**, 105–109 (2012).
17. Pfrieger, F.W. & Slezak, M. Genetic approaches to study glial cells in the rodent brain. *Glia* **60**, 681–701 (2012).
18. Sakurai, H. Targeting of TAK1 in inflammatory disorders and cancer. *Trends Pharmacol. Sci.* **33**, 522–530 (2012).
19. Adhikari, A., Xu, M. & Chen, Z.J. Ubiquitin-mediated activation of TAK1 and IKK. *Oncogene* **26**, 3214–3226 (2007).
20. Karin, M. & Gallagher, E. TNFR signaling: ubiquitin-conjugated TRAFfic signals control stop-and-go for MAPK signaling complexes. *Immunol. Rev.* **228**, 225–240 (2009).
21. Bettermann, K. *et al.* TAK1 suppresses a NEMO-dependent but NF-κB-independent pathway to liver cancer. *Cancer Cell* **17**, 481–496 (2010).
22. Sato, S. *et al.* Essential function for the kinase TAK1 in innate and adaptive immune responses. *Nat. Immunol.* **6**, 1087–1095 (2005).
23. Tang, M. *et al.* TAK1 is required for the survival of hematopoietic cells and hepatocytes in mice. *J. Exp. Med.* **205**, 1611–1619 (2008).
24. Jung, S. *et al.* Analysis of fractalkine receptor CX_3CR1 function by targeted deletion and green fluorescent protein reporter gene insertion. *Mol. Cell Biol.* **20**, 4106–4114 (2000).
25. Cardona, A.E. *et al.* Control of microglial neurotoxicity by the fractalkine receptor. *Nat. Neurosci.* **9**, 917–924 (2006).
26. Kim, K.W. *et al.* *In vivo* structure/function and expression analysis of the CX3C chemokine fractalkine. *Blood* **118**, e156–e167 (2011).
27. Geissmann, F., Jung, S. & Littman, D.R. Blood monocytes consist of two principal subsets with distinct migratory properties. *Immunity* **19**, 71–82 (2003).
28. Yona, S. *et al.* Fate mapping reveals origins and dynamics of monocytes and tissue macrophages under homeostasis. *Immunity* **38**, 79–91 (2013).
29. Dighe, A.S. *et al.* Tissue-specific targeting of cytokine unresponsiveness in transgenic mice. *Immunity* **3**, 657–666 (1995).
30. Town, T. *et al.* Blocking TGF-β–Smad2/3 innate immune signaling mitigates Alzheimer-like pathology. *Nat. Med.* **14**, 681–687 (2008).
31. Ajami, B., Bennett, J.L., Krieger, C., Tetzlaff, W. & Rossi, F.M. Local self-renewal can sustain CNS microglia maintenance and function throughout adult life. *Nat. Neurosci.* **10**, 1538–1543 (2007).
32. Mildner, A. *et al.* Microglia in the adult brain arise from Ly-6C^{hi}CCR2^{+} monocytes only under defined host conditions. *Nat. Neurosci.* **10**, 1544–1553 (2007).
33. Raasch, J. *et al.* IκB kinase 2 determines oligodendrocyte loss by non-cell-autonomous activation of NF-κB in the central nervous system. *Brain* **134**, 1184–1198 (2011).
34. van Loo, G. *et al.* Inhibition of transcription factor NF-κB in the central nervous system ameliorates autoimmune encephalomyelitis in mice. *Nat. Immunol.* **7**, 954–961 (2006).
35. Ulvestad, E. *et al.* Human microglial cells have phenotypic and functional characteristics in common with both macrophages and dendritic antigen-presenting cells. *J. Leukoc. Biol.* **56**, 732–740 (1994).
36. Sheppard, K.-A. *et al.* Transcriptional activation by NF-κB requires multiple coactivators. *Mol. Cell Biol.* **19**, 6367–6378 (1999).
37. Mildner, A. *et al.* CCR2^{+}Ly-6C^{hi} monocytes are crucial for the effector phase of autoimmunity in the central nervous system. *Brain* **132**, 2487–2500 (2009).
38. Flügel, A., Bradl, M., Kreutzberg, G.W. & Graeber, M.B. Transformation of donor-derived bone marrow precursors into host microglia during autoimmune CNS inflammation and during the retrograde response to axotomy. *J. Neurosci. Res.* **66**, 74–82 (2001).
39. Ford, A.L., Goodsall, A.L., Hickey, W.F. & Sedgwick, J.D. Normal adult ramified microglia separated from other central nervous system macrophages by flow cytometric sorting. Phenotypic differences defined and direct *ex vivo* antigen presentation to myelin basic protein-reactive CD4^{+} T cells compared. *J. Immunol.* **154**, 4309–4321 (1995).
40. Matyszak, M.K. *et al.* Microglia induce myelin basic protein-specific T cell anergy or T cell activation, according to their state of activation. *Eur. J. Immunol.* **29**, 3063–3076 (1999).
41. Wang, Y. *et al.* Transforming growth factor beta-activated kinase 1 (TAK1)-dependent checkpoint in the survival of dendritic cells promotes immune homeostasis and function. *Proc. Natl. Acad. Sci. USA* **109**, E343–E352 (2012).
42. Rajasekaran, K. *et al.* Transforming growth factor-β-activated kinase 1 regulates natural killer cell-mediated cytotoxicity and cytokine production. *J. Biol. Chem.* **286**, 31213–31224 (2011).
43. Ajibade, A.A. *et al.* TAK1 negatively regulates NF-κB and p38 MAP kinase activation in Gr-1^{+}CD11b^{+} neutrophils. *Immunity* **36**, 43–54 (2012).
44. Zehntner, S.P., Brisebois, M., Tran, E., Owens, T. & Fournier, S. Constitutive expression of a costimulatory ligand on antigen-presenting cells in the nervous system drives demyelinating disease. *FASEB J.* **17**, 1910–1912 (2003).
45. Siao, C.J., Fernandez, S.R. & Tsirka, S.E. Cell type-specific roles for tissue plasminogen activator released by neurons or microglia after excitotoxic injury. *J. Neurosci.* **23**, 3234–3242 (2003).
46. Rong, L.L. *et al.* RAGE modulates peripheral nerve regeneration via recruitment of both inflammatory and axonal outgrowth pathways. *FASEB J.* **18**, 1818–1825 (2004).
47. Jung, S. *et al.* *In vivo* depletion of CD11c^{+} dendritic cells abrogates priming of CD8^{+} T cells by exogenous cell-associated antigens. *Immunity* **17**, 211–220 (2002).

ONLINE METHODS

Mice. The generation of *Cx3cr1*^{Cre} and *Cx3cr1*^{CreER} mice has been described recently by us[28]. *Cx3cr1*^{CreER} mice were backcrossed for >9 generations onto the C57Bl/6 background. *Cx3cr1*^{Cre} mice were generated on a C57Bl/6 background. *Neo* neomycin resistance cassettes were removed by crossing the respective *Cx3cr1*^{Cre} and *Cx3cr1*^{CreER} animals with the global CMV^{Cre} deleter mouse (B6.C-Tg(CMV-cre)1Cgn/J) (Jackson Laboratories). Both *Cx3cr1*^{Cre} and *Cx3cr1*^{CreER} lines were genotyped by PCR using the forward primer 5′-CAC GGG GGA GGC AGA GGG TTT-3′ and the reverse primer 5′-GCG GAG CAC GGG CCA CAT TTC-3′, which amplify a 0.5-kb fragment from the transgenic *Cx3cr1* locus. *CD11c*^{Cre} and *LysM*^{Cre} mice were from Jackson Laboratories. Mice carrying *loxP*-site–flanked (floxed) alleles of the *Tak1* gene *Map3k7* (*Tak1*$^{fl/fl}$)[22] or *R26-yfp* mice (B6.129X1-Gt(ROSA)26Sortm1(EYFP)Cos/J) (Jackson Laboratories) were crossed to *CD11c*^{Cre}, *LysM*^{Cre}, *Cx3cr1*^{Cre}, *Cx3cr1*^{CreER} or *Nes*^{Cre} (Jackson Laboratories). For induction of Cre recombinase, 5- to 7-week-old *Cx3cr1*^{CreER} mice were treated with 4 mg tamoxifen (TAM, Sigma) solved in 200 µl corn oil (Sigma) injected subcutaneously at two time points 48 h apart or treated orally via gavage or tamoxifen-containing food[28]. In all experiments, littermates carrying the respective *loxP*-flanked alleles but lacking expression of Cre recombinase were used as controls. All animal experiments were approved by the Federal Ministry for Nature, Environment and Consumers' Protection of the state of Baden-Württemberg and were performed in accordance to the respective national, federal and institutional regulations.

Primary cultures. Cells were prepared from newborn mice as described previously[48]. For induction of Cre recombinase, OH-TAM (H7904, Sigma-Aldrich, Germany) was applied at a final concentration of 1 µM 2 to 3 d before analysis. Microglia and astrocytes were stimulated for 30 min (TNF-α) or 120 min (IL-1β, LPS) and either subsequently fixed in 4% paraformaldehyde (PFA) and processed for fluorescence microscopy or harvested in PBS for gene expression analysis.

Induction of EAE. Mice from each group were immunized subcutaneously 4 weeks after TAM injection into 8- to 12-week-old animals with 200 µg of $MOG_{35–55}$ peptide emulsified in complete Freund's adjuvant containing 1 mg of *Mycobacterium tuberculosis* (H37RA; Difco Laboratories, Detroit, Michigan, USA) . The mice received intraperitoneal injections with 250 ng pertussis toxin (Sigma-Aldrich, Deisenhofen, Germany) at the time of immunization and 48 h later.

Clinical evaluation. Mice were scored daily as follows: 0, no detectable signs of EAE; 0.5 distal limb tail; 1.0, complete limp tail; 1.5, limp tail and hindlimb weakness; 2, unilateral partial hindlimb paralysis; 2.5, bilateral partial hindlimb paralysis; 3, complete bilateral hindlimb paralysis; 3.5, complete hindlimb paralysis and unilateral forelimb paralysis; 4, total paralysis of fore- and hindlimbs.

Fluorescence microscopy. After transcardial perfusion with phosphate-buffered saline (PBS), brains were fixed in 4% PFA and embedded. 14-µm cryosections were obtained as described previously[32]. Sections were then blocked with PBS containing 5% bovine serum albumin and permeabilized with 0.1% Triton X-100 in blocking solution. Primary antibodies were added overnight at a dilution of 1:500 for Iba-1 (019-19741, WACO, Japan)[49], 1:1,000 for GFP (600-106-215, Rockland Immunochemicals Inc., Gilbertsville, USA)[50], 1:100 for rhodamine-labeled isolectin B4 (RL-1102, Vector Laboratories, Burlingame, USA)[50], 1:500 for GFAP (Z0334, Dako, Hamburg, Germany)[51], 1:200 for NeuN (mab377, EMD Millipore, Billerica, MA, USA)[51], 1:250 for LAMP-2 (ab13524, Abcam, Cambridge, UK)[50], 1:100 for MHC class II (ab23990, Abcam)[50], 1:100 for p65 (sc-372, Santa Cruz Biotechnologies, Dallas, USA)[51], 1:100 for Lys310-acetylated p65 (ab52175, Abcam)[52], 1:100 for phospho-JNK (9255S, Cell Signaling, Danvers, USA)[53], 1:100 for phospho-ERK1/2 (sc-101761, Santa Cruz)[54] and 1:100 for phospho-p38 (9215S, Cell Signaling)[55] at 4 °C. Secondary antibodies were added as follows: Alexa Fluor 488, 1:500; Alexa Fluor 555, 1:500; Alexa Fluor 568, 1:500, for 2 h at room temperature. Nuclei were counterstained with DAPI. GFP-expressing and Iba-1$^+$ macrophages were counted in at least three sections of each animal according to earlier protocols[32,49]. The number of cells and the examined area were determined microscopically using a conventional fluorescence microscope (Olympus BX-61) and the confocal pictures were taken with Fluoview FV 1000 (Olympus).

Three-dimensional reconstruction of microglia. Free-floating 30-µm cryosections from adult brain tissue were stained overnight with anti-Iba-1 (1:500) at 4 °C, followed by Alexa Fluor 568–conjugated secondary antibody at a dilution of 1:500 for 2 h at 20–25 °C. Nuclei were counterstained with DAPI. Imaging was performed on an Olympus Fluoview 1000 confocal laser scanning microscope using a 20× 0.95 NA objective. *z*-stacks with 1.1-µm steps in the *z* direction, 1,024 × 1,024 pixel resolution, were recorded and analyzed using Imaris software (Bitplane).

Histology. Histology was performed as described recently[56]. Spinal cords were removed on day 25 after immunization and fixed in 4% buffered formalin. Then spinal cords were dissected and embedded in paraffin before staining with H&E, Luxol fast blue to assess the degree of demyelination, MAC-3 (1:200, BD Pharmingen)[56] for macrophages and microglia, CD3 (1:100, MCA1477 Serotec, Düsseldorf, Germany)[56] for T cells, B220 (1:200, BD Pharmingen) for B cells and APP (1:3,000, MAB348, Millipore)[56] for indication of axonal damage (Serotec, Düsseldorf, Germany). Spinal cord sections were evaluated using cell-P software (Olympus).

Flow cytometry. Cells were stained with primary antibodies directed against B220 (RA3-6B2)[56], CD3 (17A2)[56], CD11b (M1/70)[56], CD45 (30-F11)[56], CD115 (AFS98)[56], CD8 (SK1)[56] (eBioscience, San Diego, USA), CD4 (RM4-5)[56], Ly6C (AL-21)[56], MHC class II (2G9)[56] (BD Biosciences, Heidelberg, Germany) and NKp46 (BioLegend, San Diego, USA)[56] all diluted 1:20 at 4 °C for 15 min. Cells were washed and analyzed using a FACSCanto II (Becton Dickinson) flow cytometer. Viable cells were gated by forward and side scatter pattern. Data were acquired with FACSdiva software (Becton Dickinson). Post-acquisition analysis was performed using FlowJo software (Tree Star, Inc.).

Recall assay. On day 7, the draining axillary and inguinal lymph nodes (LN) were removed from $MOG_{35–55}$-immunized mice and single-cell suspensions were prepared. 6×10^5 LN cells were placed as triplicates in a 96-well plate and pulsed with the indicated dosages of MOG peptide. BrdU uptake was measured for 16 h to determine proliferation (Cell Proliferation ELISA colorimetric, Roche Applied Science) according to the manufacturer's protocol. RPMI 1640 (Invitrogen) and Dulbecco's modified Eagle's medium (Invitrogen) each supplemented with 10% (v/v) FCS, 3 mM L-glutamine, 100 U/ml penicillin and 100 µg/ml streptomycin (all from Sigma-Aldrich) were used. For cytokine analysis, sister cultures supernatants were analyzed by ELISA for IFN-γ and IL-17 (R&D Systems, Wiesbaden, Germany).

qRT-PCR. Tissues were dissected and flushed with ice-cold HBSS. RNA was isolated using the RNeasy Mini Kit (Qiagen, Hilden, Germany) following the manufacturer's instructions. Samples were treated with DNaseI (Roche, Mannheim, Germany) and 1.5 µg of RNA was transcribed into cDNA using oligo(dT) primers and the SuperScript II RT kit (Invitrogen, Carlsbad, CA). 1 µl cDNA was transferred into a 96-well Multiply PCR plate (Sarstedt, Germany) with 11.5 µl ABsolute QPCR SYBR Green master mix (Thermo Fisher). RT-PCR reactions were performed as described recently[49,56].

Western blot analysis and histone extraction. Tissues or cells were extracted in RIPA buffer (25 mM Tris-HCl, 150 mM NaCl, 1% Nonidet P-40, 0.5% sodium deoxycholate, 0.1% SDS, pH 7.5). Samples were separated by SDS-PAGE and immunoblotted using antibodies to TAK1 (1:500, sc-7162, Santa Cruz)[57], Lys310-acetylated p65 (1:500, Abcam)[52], phospho-JNK (1:500, Cell Signaling)[53], phospho-p38 (1:500, Cell Signaling)[54] and Gapdh (1:2,500, Mab374, Millipore, Billerica, USA)[51]. For histone extraction, cells were harvested and washed twice in ice-cold PBS containing 5 mM sodium butyrate. Cell lysis and isolation of nuclei was then performed in PBS containing 0.5% Triton X-100, 2 mM phenylmethylsulfonyl fluoride and 0.02% (w/v) NaN_3. Histones were extracted from the isolated nuclei through acid extraction in 0.2 N HCl overnight at 4 °C. Western blot analysis was performed on the extracted histones using antibodies directed against histone H3 (1:4,000, D1H2, Cell Signaling)[58] and histone H3 acetylated at Lys9 (H3K9ac; 1:4,000, ab10812, Abcam)[58].

Statistics and general methods. For the sample size in EAE experiments, power analysis was performed. A sample size of at least $n = 15$ per group was determined by 80% power to reach statistical significance of 0.05 to detect an effect size of at least 1.06. To obtain unbiased data, experimental mice of all relevant genotypes were all processed together by technicians and cell quantifications were performed blinded to the genotype by two scientists independently and separately. Only after finalization of all quantitative measurements were the samples allocated to their genotypes.

There was no randomization of mice or samples before analysis. Therefore, all samples or mice were included in our analysis.

Significance of clinical EAE scores was evaluated using the Mann-Whitney *U* test. For statistical analysis of all other experiments, all data were tested for normality applying the Kolmogorov-Smirnov test. If normality was given, an unpaired *t*-test was applied. If the data did not meet the criteria of normality, the Mann-Whitney *U* test was applied. Differences were considered significant when the *P* value was <0.05.

48. Prinz, M. & Hanisch, U.K. Murine microglial cells produce and respond to interleukin-18. *J. Neurochem.* **72**, 2215–2218 (1999).
49. Mildner, A. *et al.* Distinct and non-redundant roles of microglia and myeloid subsets in mouse models of Alzheimer's disease. *J. Neurosci.* **31**, 11159–11171 (2011).
50. Kierdorf, K. *et al.* Microglia emerge from erythromyeloid precursors via Pu.1- and Irf8-dependent pathways. *Nat. Neurosci.* **16**, 273–280 (2013).
51. Raasch, J. *et al.* IκB kinase 2 determines oligodendrocyte loss by non-cell-autonomous activation of NF-κB in the central nervous system. *Brain* **134**, 1184–1198 (2011).
52. Clavijo, P.E. & Frauwirth, K.A. Anergic CD8+ T lymphocytes have impaired NF-κB activation with defects in p65 phosphorylation and acetylation. *J. Immunol.* **188**, 1213–1221 (2012).
53. Bond, D., Primrose, D.A. & Foley, E. Quantitative evaluation of signaling events in Drosophila S2 cells. *Biol. Proced. Online* **10**, 20–28 (2008).
54. Atif, F. *et al.* Combination treatment with progesterone and vitamin D hormone is more effective than monotherapy in ischemic stroke: the role of BDNF/TrkB/Erk1/2 signaling in neuroprotection. *Neuropharmacology* **67**, 78–87 (2013).
55. Wolf, M.J. *et al.* Endothelial CCR2 signaling induced by colon carcinoma cells enables extravasation via the JAK2-Stat5 and p38MAPK pathway. *Cancer Cell* **22**, 91–105 (2012).
56. Dann, A. *et al.* Cytosolic RIG-I-like helicases act as negative regulators of sterile inflammation in the CNS. *Nat. Neurosci.* **15**, 98–106 (2012).
57. Bettermann, K. *et al.* TAK1 suppresses a NEMO-dependent but NF-κB-independent pathway to liver cancer. *Cancer Cell* **17**, 481–496 (2010).
58. Ngubo, M., Kemp, G. & Patterton, H.G. Nano-electrospray tandem mass spectrometric analysis of the acetylation state of histones H3 and H4 in stationary phase in *Saccharomyces cerevisiae*. *BMC Biochem.* **12**, 34 (2011).